Advanced Modeling of Gas Compressors for Globally Convergent Stationary Network Solvers

Tanja Clees, Igor Nikitin, Lialia Nikitina
Fraunhofer Institute for Algorithms and Scientific Computing
Sankt Augustin, Germany
Email: {Tanja.Clees|Igor.Nikitin|Lialia.Nikitina}@scai.fraunhofer.de

***Abstract*—The simulation of transport networks in civil engineering has become increasingly important for the planning and stable operation of modern infrastructure. Compressors are essential elements in gas transport networks; they create pressure necessary for driving gas towards the consumers. This paper presents mathematical modeling of gas compressors, taking into account their individually calibrated physical profiles. The approach is based on conversion of the measured profiles into an explicitly resolved form suitable for globally convergent solvers. In particular, a proper signature of derivatives for the element equation of a compressor is provided. The usability of the approach is demonstrated on a number of real-life network scenarios.**

Keywords–modeling of complex systems; globally convergent solvers; applications; gas transport networks.

I. INTRODUCTION

In our previous paper [1], it has been shown that specific solvers for generic stationary network problems can be made globally convergent under special conditions on modeling of their elements. Stationary network problems combine linear Kirchhoff's equations and (generally non-linear) element equations. The first class of equations represents conservation laws, the second class describes transport. We have shown that under certain monotonicity conditions on element equations, i.e., a special signature of the derivatives, the whole system possesses a globally non-degenerate Jacobi matrix. As a result, the problem always has exactly one solution. Moreover, standard algorithms, like Armijo backtracking line search and Katzenelson piecewise linear tracing, provide convergence to this solution from an arbitrary starting point.

These ideas have been implemented in our multi-physics network simulator MYNTS as described in [2], [3]. Considering gas transport networks, these papers used a simplified modeling of gas compressors, known in the simulation community as *free compressors*. This type of compressors does not possess limits on their power, only input or output pressure or gas flow are restricted. The present work extends the modeling by realistic characteristics to so called *advanced compressors*. Such compressors are described by individually measured physical profiles, defining the limits on power, revolution number, working region, etc. We will show how to incorporate such realistic characteristics into our globally convergent solver.

Modeling of gas transport networks has been considered in full detail in paper [4]. The networks are composed of a variety of elements (pipes, valves, compressors, drives, regulators, resistors, etc.), each type possessing a particular element equation. For instance, the pressure drop in pipes is described either by an empiric quadratic law [5] or by more accurate formulae by Nikuradse [6] and Colebrook-White [7]. Compressors and regulators have a control logic, implemented in the form of control equations or inequalities [4], e.g., a compressor/regulator can have a control goal to keep fixed output pressure, input pressure or flow value. There are various models for compressors (turbo, piston) and their drives (gas turbine, steam turbine, gas motor, electro motor), with characteristic diagrams calibrated on real engines.

The nodal variables (pressure, density, temperature, etc.) are related by equations of state, including various gas laws (ideal, Papay, standards of the American Gas Assotiaciation – AGA and the International Organization for Standardization – ISO [8], [9]). Gas composition is defined in terms of molar components and effective gas properties (critical temperature and pressure, calorific value, molar mass, etc.), with appropriate equations describing their propagation and mixing. Thermal modeling [4] includes a number of physical effects (non-linear heat capacity, heat exchange with the soil, Joule-Thomson effect, i.e., a temperature drop due to free expansion of gas through a valve, regulator, etc.).

The obtained system of equations and inequalities is solved by non-linear programming methods [10], [11]. Due to the non-linearity of equations, the stability of the solver critically depends on the choice of the starting point. For this purpose, various empirical strategies are used [12], [13]. An alternative has been proposed in our papers [1], [2], employing globally convergent algorithms, able to find the solution from an arbitrary starting point.

In Section II, we recall conditions on the generic stationary network problem, necessary for global convergence, and concretize these conditions in application to gas transport networks. In Section III, we introduce advanced gas compressors. In Section IV, we present our implementation of advanced compressor modeling which fulfills the conditions for global convergence. In Section V, we apply the respective realization in MYNTS to a number of realistic gas transport network examples and discuss the results obtained.

MYNTS is a cross-platform application, available on request from [14].

II. GLOBAL CONVERGENCE AND GAS TRANSPORT NETWORKS

A generic stationary network problem can be written as

$$\sum_e I_{ne} Q_e = Q_n^{(s)},\ n \notin N_P,\ P_n = P_n^{(s)},\ n \in N_P,$$
$$f_e(P_{in}, P_{out}, Q_e) = 0, \qquad (1)$$

 ISBN: 978-1-61208-567-8

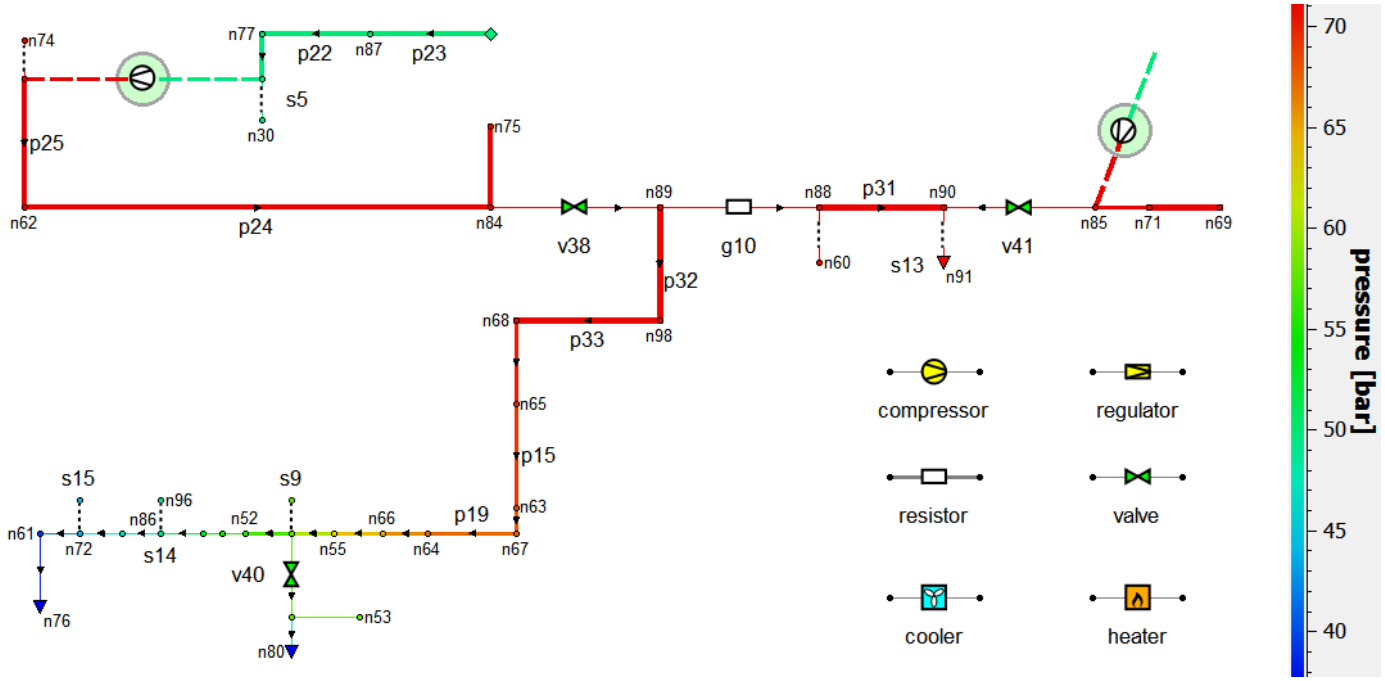

Figure 1. Test gas transport network N1 with 100 nodes, 111 edges.

where indices $n = 1...N$ denote the nodes and $e = 1...E$ the edges of the associated network graph, I_{ne} is an incidence matrix of the graph, Q_e are flows through the edges, $Q_n^{(s)}$ are source/sink contributions, localized in supply/exit nodes, P_n are nodal variables (pressure for gas transport networks), $P_n^{(s)}$ are set values, localized in the subset N_P of supply/exit nodes, at least one value per connected component of the graph. Let the element equations possess derivatives of the signature:

$$\partial f_e/\partial P_{in} > 0,\ \partial f_e/\partial P_{out} < 0,\ \partial f_e/\partial Q_e < 0. \quad (2)$$

It has been proven in [1] that the system (1) under condition (2) possesses a globally non-degenerate Jacobi matrix.

Gas transport networks, e.g., the networks shown in Figure 1, consist of several types of elements, all possessing the property (2). The gas networks are mostly composed of pipes with a non-linear (nearly quadratic) element equation. Some elements (valves and shortcuts) have linear equations, but most complex elements (compressors and regulators) possess piecewise linear equations. According to [13], all continuous piecewise linear functions can be represented in a max-min form:

$$f(x) = \max_i \min_j \sum_k a_{ijk} x_k + b_{ij}, \quad (3)$$

where a, b are coefficient lists. In particular, free compressors are described by the following element equation:

$$\begin{aligned} &\max(\min(\ P_{in} - \epsilon P_{out} - \epsilon Q - P_L, \quad (4)\\ &\epsilon P_{in} - P_{out} - \epsilon Q + P_H, \epsilon(P_{in} - P_{out}) - Q\\ &+Q_H), P_{in} - P_{out} - \epsilon Q, \epsilon(P_{in} - P_{out}) - Q) = 0. \end{aligned}$$

The compressor tries to satisfy one of the following control goals: a specified pressure on output (SPO), a specified pressure on input (SPI) or a specified mass flow (SM). Being combined with the given upper and lower bounds: $PH = \min(SPO, POMAX)$, $PL = \max(SPI, PIMIN)$, $QH = \min(SM, MMAX)$, the element equation defines a polyhedral surface shown in Figure 2, top. Here, PH stands for high pressure limit, PL – low pressure limit, QH – high flow limit; $POMAX$ is an upper safety bound on output pressure, $PIMIN$ is a lower safety bound on input pressure, $MMAX$ is an upper safety bound on the flow. Every face of the diagram corresponds to the best possible satisfaction of the control goal, e.g., $P_{out} = PH$ (typical for SPO-mode), $Q = QH$ (typical for SM-mode), $P_{in} = P_{out}$ (bypass BP, equivalent to an open valve), $Q = 0$ (OFF, equivalent to a closed valve), etc. A small ϵ value is used for regularization purposes. Every compressor is part of a compressor station, the simplest one is shown on Figure 2, bottom. This figure presents a compressor station with one machine unit, including (in flow direction) input resistor, compressor, cooler, output resistor, exit valve, (in an oblique direction) bypass valve, bypass regulator, both currently closed. In more complex stations, the compressors with accompanying elements are cascaded to parallel or sequential configurations.

III. Advanced Modeling of Gas Compressors

In addition to pressure P, the nodes in gas transport networks possess other common variables, including: ρ – mass density, T – temperature, z – compressibility factor, μ – molar mass. In addition to conserving mass flow Q, measured in kg/s, sometimes volume flow Q_x is also considered. It is measured in m^3/s with explicit reference to the measurement conditions, e.g., Q_{norm} represents the volume flow under normal conditions (1 bar, 273.15 K), $Q_{in,out}$ refers to the volume flow under conditions in the input and output nodes. Different flow definitions are related by the formula:

$$Q = Q_{norm}\rho_{norm} = Q_{in}\rho_{in} = Q_{out}\rho_{out}. \quad (5)$$

 ISBN: 978-1-61208-567-8

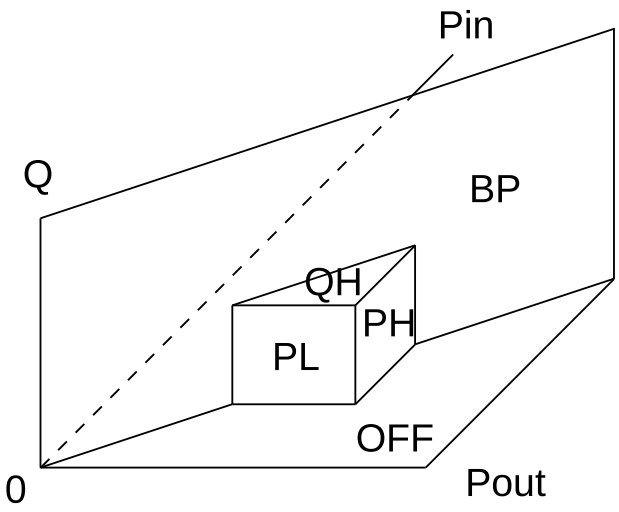

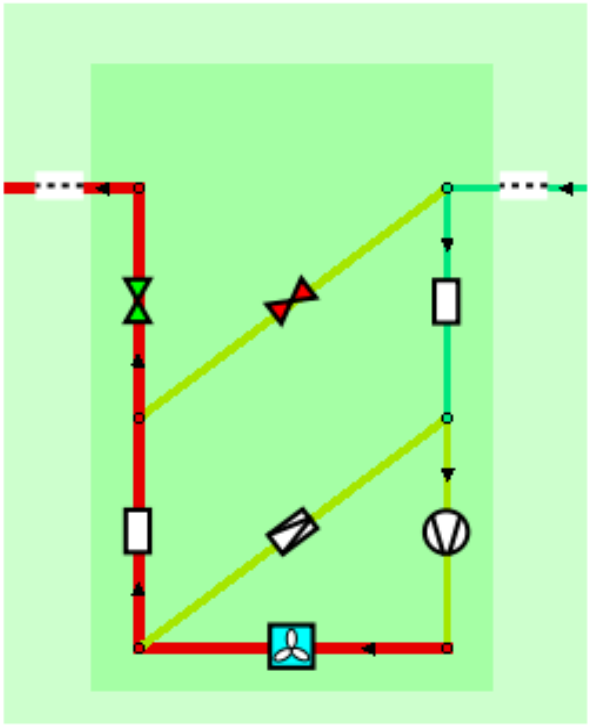

Figure 2. On the top: control diagram of free compressor. On the bottom: a compressor station with one typical machine unit.

Advanced compressors bring four new variables: H_{ad} – adiabatic enthalpy increase, η_{ad} – adiabatic efficiency, r – revolution number of compressor drive, W – power of compressor drive. Also, four equations are added [4]:

$$\begin{aligned} &H_{ad} = RT_{in}z_{in}/(\mu\alpha)\cdot((P_{out}/P_{in})^{\alpha}-1)\,,\\ &W = QH_{ad}/\eta_{ad},\\ &H_{ad} = (1,r,r^2)\cdot A\cdot(1,Q_{in},Q_{in}^2)^T,\\ &\eta_{ad} = (1,r,r^2)\cdot B\cdot(1,Q_{in},Q_{in}^2)^T, \end{aligned} \tag{6}$$

where R is the universal gas constant, κ the adiabatic exponent, $\alpha = (\kappa-1)/\kappa$. A and B are (3x3)-matrices filled with calibration constants. In addition, working limits for compressors are defined by the following inequalities:

$$\begin{aligned} &r_{min} \le r \le r_{max},\ \eta_{ad} \ge \eta_{min},\\ &Q_{in} \ge Q_{min},\ W \le W_{max},\\ &Q_{min} = (1, H_{ad}, H_{ad}^2)\cdot C^T,\\ &W_{max} = (1, r, r^2)\cdot D^T, \end{aligned} \tag{7}$$

where the constants r_{min}, r_{max} define limits of the revolution number, η_{min} – the lower limit on efficiency (so called choke line; Q_{min} is a lower limit on the input volume flow (a surge line), W_{max} is an upper limit on power. C, D are (3)-vectors filled with calibration constants.

The constants in (A, B, C, D) are found by fitting the measured data for the compressor considered as part of a calibration procedure and further represent the individual profiles for this compressor. Here, we described the modeling for a common class of turbo compressors and gas turbine drive engines. The other types are simpler in implementation and can be modeled analogously.

Figure 3 (top) shows profiles for a typical turbo compressor. In this plot, the horizontal axis represents input volume flow Q_{in}, the vertical axis – adiabatic enthalpy increase H_{ad}. Solid blue curves are the lines of constant revolution number r, their uppermost curve corresponds to r_{max}, the lowest curve – to r_{min}. The red curve is the surge line $Q_{in} = Q_{min}$, while the rightmost green curve – the choke line $\eta_{ad} = \eta_{min}$. The points in this diagram depict the data measured, a blue cross denotes the current working point of the compressor.

The equations (6) serve as definitions of newly introduced variables, while the inequalities (7) define the restrictions, in addition to (4) of those for a free compressor. The upper bounds $r = r_{max}$ and $W = W_{max}$ define new upper bounds for the flow and should be combined with the one defined by the diagram for a free compressor, shown in Figure 2 top. The lower bounds $r = r_{min}$ and $Q_{in} = Q_{min}$ show the points where the station automatically opens its bypass regulator, shown in Figure 2 bottom. After that the gas starts to circulate inside the station, so that the compressor never violates its bounds. The choke line $\eta_{ad} = \eta_{min}$ cuts off a region of unstable calibration related with the small η_{ad} in the denominator of (6). Usually, the working point of a compressor is not located in this region, except of the starting procedure. On necessity the diagram can be continued in this region by a convenient monotone formula.

If P_{in} and P_{out} are fixed and the compressor is on its $r = r_{max}$ limit, it is straightforward to resolve the equations analytically, finding H_{ad}, Q_{in}, ρ_{in}, Q, η_{ad} and W, in this order. If r and Q_{in} are fixed and the compressor is on its $W = W_{max}$ limit, the equations can be resolved in the order H_{ad}, η_{ad}, W_{max}, Q, ρ_{in}, P_{in}, P_{out}. The first analytic formula gives an explicit representation $Q(P_{in}, P_{out})$ for the surface, defining a patch of the element equation. The second one represents the other patch in a parametric form $(r, Q_{in}) \to (P_{in}, P_{out}, Q)$. By numerical differentiation, it is possible to find the normals to both surfaces, which directly define the signatures of the corresponding patches. We recall that the correct signature reads $(+--)$, see (2). In Figure 3 (bottom) green points show the area of wrong signature. The

 ISBN: 978-1-61208-567-8

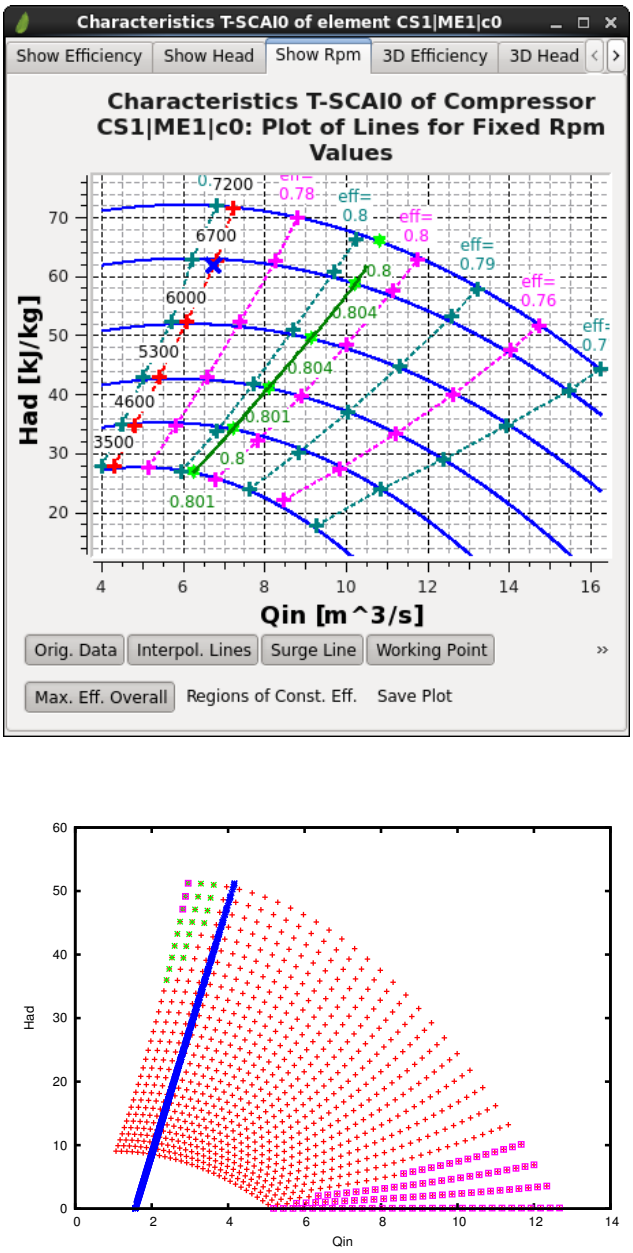

Figure 3. Advanced modeling of compressors. On the top: typical characteristic diagram. Solid blue curves are lines of constant revolution number. On the bottom: stability analysis.

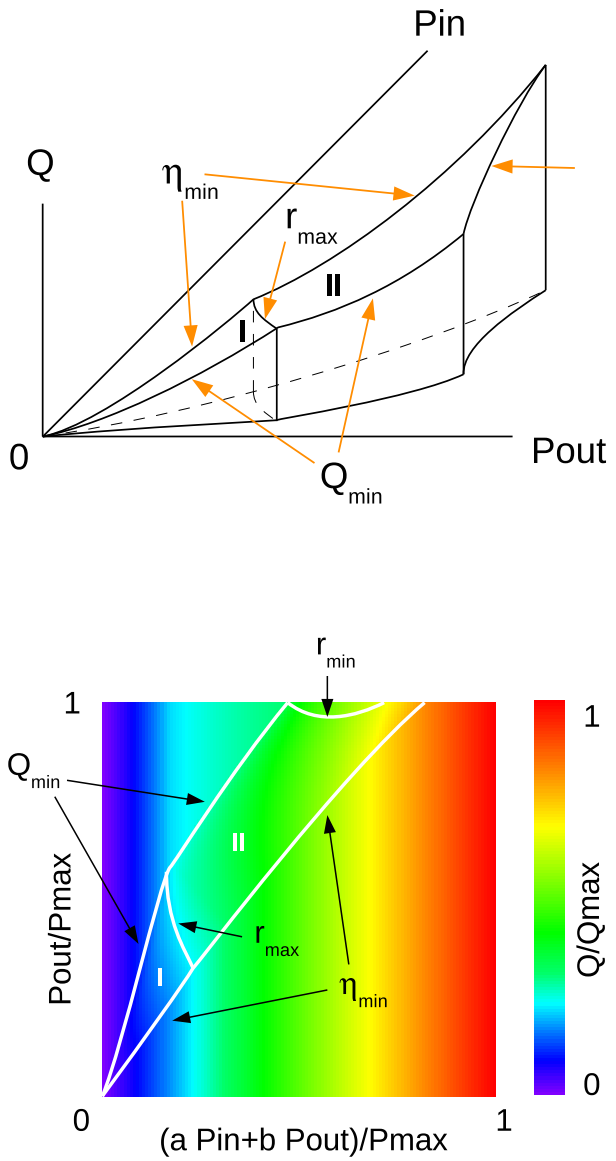

Figure 4. Advanced modeling of compressors (cont'd). On the top: control diagram of an advanced compressor. On the bottom: the same diagram in affine coordinates and color map representation.

blue curve is the surge line, magenta points show the area $\eta_{ad} < \eta_{min}$. Normally, the unstable green area is cut off by the surge and choke lines, so that the whole working region of the compressor is stable. In rare cases, when it is not so, the surge and choke lines should be modified accordingly.

IV. Globally convergent implementation

Figure 4 (top) shows the surface $Q_{adv}(P_{in}, P_{out})$ defined by the characteristics of the advanced compressor. The calibrated part of the surface is located between the curves Q_{min} and η_{min} and consists of two patches I and II, connected on the r_{max} line. Patch I is located between the r_{max} line and the origin. Here, the input and output pressures are small and the compressor's performance is limited by its maximal revolution number: $r = r_{max}$. Patch II is located between the r_{max} and r_{min} lines. Here, the pressures are large and the compressor is limited by the maximal power of the drive: $W = W_{max}$. On Q_{min} and r_{min} curves the surface vertically falls down. This behavior corresponds to the open bypass regulator. Q in that case denotes a total mass flow through the compressor and bypass regulator. The flow through the compressor remains equal to Q_{min} or the equivalent flow on the r_{min} line, while the negative difference ΔQ circulates through the bypass regulator. A slope of the vertically falling faces should be ϵ-regularized to provide the necessary signature $(+\,-\,-)$. The surface should be continued beyond η_{min} curve by any function supporting the same signature.

Figure 4 (bottom) shows the same diagram as a color map. Patch II requires a conversion from parametric to explicit rep-

resentation. For this purpose, we adopt resampling algorithms well known in computer graphics (CG). At first, we perform an affine transformation:

$$\begin{pmatrix} x \\ y \end{pmatrix} = \begin{pmatrix} a & b \\ 0 & 1 \end{pmatrix} \begin{pmatrix} P_{in} \\ P_{out} \end{pmatrix} \cdot \frac{1}{P_{max}}, \qquad (8)$$

with $a + b = 1$. The square on the (x, y)-plane is represented as a $N_{px} \times N_{px}$ pixel buffer, storing floating point values of Q in double precision. Patches I and II are regularly sampled and represented as triangle strip sets. Then, the patches are rendered onto the (x, y)-plane using the Z-buffer algorithm. Finally, the remaining gaps are filled by copying a constant Q-value along the columns and to the right – by a linearly increasing function in the row. As a result, the Q_{adv}-function in these regions becomes dependent only on x. Monotonous increase of Q on the border lines and a choice of affine coefficients $a > 0$, $b < 0$ support correct signature of the function $Q_{adv}(P_{in}, P_{out})$. If the bypass regulator is activated, the part above the upper border lines must be reset towards $Q = 0$, providing a regularized vertical fall of the surface on this bound.

The described algorithms provide a transformation from the calibration coefficients (A, B, C, D) and characteristic diagram in Figure 3 (top) to the tabulated function $Q_{adv}(P_{in}, P_{out})$, represented by the color map in Figure 4 (bottom). This transformation should be done once per advanced compressor. For a moment, we use an implementation of the CG algorithms on Central Processing Unit (CPU) and plan their acceleration with Graphics Processing Unit (GPU).

In the solver, the lookup function $Q_{adv}(P_{in}, P_{out})$ is made available via rapid bilinear interpolation of tabulated values inside the (x, y)-square. It is continued to the whole (x, y)-plane by an explicit analytic formula:

$$f(x, y) = f(\hat{x}, \hat{y}) + k(\min(x, 0) + \max(x - 1, 0)), \quad (9)$$
$$\hat{x} = \min(\max(x, 0), 1), \ \hat{y} = \min(\max(y, 0), 1),$$

with a constant $k > 0$. This global function is constructed similarly to the continuation formulas in [1]. In our special case it provides monotonous increase in x and constancy in y outside of the tabulated region.

Finally, the element equation for an advanced compressor is obtained by extending (4) as follows:

$$\begin{aligned} &\max(\min(\ P_{in} - \epsilon P_{out} - \epsilon Q - P_L, \qquad (10)\\ &\epsilon P_{in} - P_{out} - \epsilon Q + P_H, \underline{Q_{adv}(P_{in}, P_{out}) - Q},\\ &\epsilon(P_{in} - P_{out}) - Q + Q_H), P_{in} - P_{out} - \epsilon Q,\\ &\epsilon(P_{in} - P_{out}) - Q) = 0. \end{aligned}$$

For clarity, the inserted term is underlined.

We have implemented the algorithms described above in our network simulator MYNTS in a preliminary version (solver strategy "stable").

V. RESULTS

For benchmarking the algorithms, we have received a number of realistic test scenarios from our partners. The simplest gas transport network N1 from our test set is shown in Figure 1. It contains two compressor stations, each equipped with two machine units, cf. Figure 2 (bottom), working in parallel mode. It has two supplies and three major consumers. The color shows the pressure distribution over the network, arrows – the direction of gas flow, thickness of lines – the diameter of the pipes. Supplies are shown by rhombi, consumers (n76, n80, n91) are shown by triangles. The main elements are shown in the legend.

A closeup to one of the compressors is shown in Figure 2 (bottom), and its characteristics are displayed in Figure 3 (top). Parameters of more complex networks are presented in Table I. In particular, medium-sized network N2 contains about a thousand nodes and edges and is equipped with 7 compressors. The largest considerd network N3 has about five thousand nodes and edges and is driven by 25 compressors. Topological connection of elements in the network together with geographic coordinates, the lengths and diameters of pipes form so called *geometry* of the network. Physical setting, such as supply pressures and consumer flows, control settings of compressors and regulators, define *scenario* for the particular simulation case. All networks in our test set were simulated with the same gas composition at 20°C environmental temperature.

TABLE I. PARAMETERS OF TEST NETWORKS

network	nodes	edges	compressors
N1	100	111	4
N2	931	1047	7
N3	4466	5362	25

In Table II, we compare the performance of the newly implemented algorithms (strategy "stable") with the performance of the solver with standard settings. For each network in the test set two scenarios are considered, with different numerical values of set points for input pressures and output flows and compressor/regulator SM, SPO settings. Divergent cases are marked as 'div'. The number of iterations (iter.) and timing (t) are given. The simulation is performed on a 3 GHz Intel i7 CPU 8 GB RAM workstation.

TABLE II. COMPARISON OF THE ALGORITHMS

scenario	solver_strategy							
	standard				stable			
	free		advanced		free		advanced	
	iter.	t, sec	iter.	t, sec	iter.	t, sec	iter.	t, sec
N1S1	3	0.01	32	0.12	2	0.01	2	0.01
N1S2	57	0.17	70	0.21	11	0.03	4	0.02
N2S1	11	0.27	19	0.64	12	0.31	12	0.37
N2S2	div	–	div	–	13	0.36	15	0.48
N3S1	div	–	div	–	26	3.3	23	3.5
N3S2	47	6.5	div	–	26	3.3	24	3.6

All scenarios are tested both with free and advanced compressor models. We see that the standard solver provides worse

 ISBN: 978-1-61208-567-8

convergence and even diverges in certain scenarios. Some scenarios show divergence already for free compressors, some diverge on advanced ones only. The new algorithm converges in all cases, in agreement with its theoretical properties. We also see that the table lookup implemented for advanced modeling has a negligible computational overhead in strategy "stable".

VI. Conclusion

In this paper, we presented mathematical modeling of gas compressors with their individually calibrated physical profiles. The measured profiles are converted to an explicitly resolved form using algorithms inspired by computer graphics. The control element equation for a free compressor has been extended by a lookup function representing the working region of the advanced compressor. The resulting equation possesses the desired signature of derivatives necessary for global non-degeneracy of the Jacobi matrix. As a result, the globally convergent algorithm developed for the solution of network problems with free compressors remains applicable, with a negligible computational overhead. The usability of the approach has been demonstrated for a number of real-life network scenarios. The algorithm significantly overperforms a standard Newtonian solver in terms of stability, number of iterations and computational time.

Acknowledgment

This work is supported by German Federal Ministry for Economic Affairs and Energy, project BMWI-0324019A, MathEnergy: Mathematical Key Technologies for Evolving Energy Grids.

References

[1] T. Clees, I. Nikitin, L. Nikitina, "Making Network Solvers Globally Convergent", in Advances in Intelligent Systems and Computing, Springer, 2017 (in print).

[2] T. Clees, N. Hornung, I. Nikitin, L. Nikitina, "A Globally Convergent Method for Generalized Resistive Systems and its Application to Stationary Problems in Gas Transport Networks", In Proc. SIMULTECH 2016, SCITEPRESS, 2016, pp. 64-70.

[3] T. Clees et al., "MYNTS: Multi-phYsics NeTwork Simulator", In Proc. SIMULTECH 2016, SCITEPRESS, 2016, pp. 179-186.

[4] M. Schmidt, M. C. Steinbach, B. M. Willert, "High detail stationary optimization models for gas networks", Optimization and Engineering, vol. 16, num.1, 2015, pp. 131-164.

[5] J. Mischner, H.G. Fasold, K. Kadner, System-planning basics of gas supply, Oldenbourg Industrieverlag GmbH, 2011 (in German).

[6] J. Nikuradse, "Laws of flow in rough pipes", NACA Technical Memorandum 1292, Washington, 1950.

[7] C. F. Colebrook and C. M. White, "Experiments with Fluid Friction in Roughened Pipes", in Proc. of the Royal Society of London, Series A, Mathematical and Physical Sciences, vol. 161, num. 906, 1937, pp. 367-381.

[8] J. Saleh, ed., Fluid Flow Handbook, McGraw-Hill Handbooks, McGraw-Hill, 2002.

[9] DIN EN ISO 12213-2: Natural Gas – Calculation of compression factor, European Committee for Standartization, 2010.

[10] A. Wächter and L. T. Biegler, "On the implementation of an interior-point filter line-search algorithm for large-scale nonlinear programming", Mathematical Programming, vol. 106, num. 1, 2006, pp. 25-57.

[11] R. Fletcher, Practical Methods of Optimization, Wiley, 2013.

[12] M. Schmidt, M. C. Steinbach, B. M. Willert, "High detail stationary optimization models for gas networks: validation and results", Optimization and Engineering online, 2015, DOI: 10.1007/s11081-015-9300-3

[13] A. Griewank, J.-U. Bernt, M. Radons, T. Streubel, 'Solving piecewise linear systems in abs-normal form", Linear Algebra and its Applications, vol. 471, 2015, pp. 500-530.

[14] Multiphysical Network Simulator MYNTS, www.scai.fraunhofer.de/en/products.html

 ISBN: 978-1-61208-567-8